Light Scattering Studies on the Crystallization Transition of Native and Per-2,6-dimethylated β-Cyclodextrins

Patrick Umbach, Yannis Georgalis,* and Wolfram Saenger

Contribution from the Institut für Kristallographie, Freie Universität Berlin, Takustrasse 6, 14195 Berlin, Germany

Received February 21, 1996[⊗]

Abstract: The initial crystallization phase of native and dimethylated β-cyclodextrins (β-CD) was investigated with small-angle static light scattering. Following simple considerations, one can obtain the crystallization exponent, predicted by the Avrami theory, from temperature quenching experiments. We found that a single-step mechanism, in accordance with the classical theory, holds for the crystal formation of native β-cyclodextrin. The crystal formation mechanism of the heptakis(2,6)-di-*O*-methyl)-β-CD is more complex, and involves a fast and a slow process. The exponents determined for each process indicate that crystallization starts with the formation of spherical clusters which aggregate further to form rod-shaped macrocrystals, in accordance with microscopic observations. In either case the determined exponents depend on the initial cyclodextrin concentration.

Introduction

Cyclodextrins (hereafter abbreviated as CD) are a family of four cyclic oligosaccharides, α, β, γ, and δ, comprising six to nine $\alpha(1-4)$-linked glucopyranose units, respectively.[1−3] They form inclusion compounds with molecules that fit in their central cavity, which is of wide practical importance in the pharmaceutical industry. CDs have also been used as building blocks of devices for chemically modulating biological activity, in particular through photochemical reactions. Such functions can suit molecular scale devices.[4] Besides "native" CDs, a variety of derivatives with chemically modified O2H, O3H, and/or O6H hydroxyl groups are available.

CDs crystallize readily as "empty" hydrates or as inclusion complexes if hot, supersaturated, aqueous solutions of CD with or without added guest molecules are slowly cooled to ambient temperature. Because of the different crystal packing forms,[5,6] CDs are attractive for studying the crystallization of simple binary or ternary systems. In this work we have investigated the properties of β-CD-11H_2O, which is the least soluble of all CDs in water at ambient temperature as well as of a modified form, heptakis(2,6-di-*O*-methyl)-β-CD (hereafter abbreviated as DIMEB), which in contrast to native β-CD is very soluble in water at ambient temperatures and crystallizes upon heating.

In earlier works, cluster formation of CD hydrates and inclusion complexes was investigated by turbidity[7] and light scattering measurements.[8] In the present study we have employed a home-built small-angle static light scattering (SLS) device to investigate the nucleation process in aqueous solutions of native β-CD and DIMEB.

Light scattering yields information concerning the size and shape of the growing clusters in a nondestructive manner. In conventional SLS equipment, the angular range is usually limited between 15° and 160°. This range allows, especially for aqueous solutions, without many problems the determination of the particle scattering function for ensembles of particles that are comparable in size with the wavelength of the employed radiation. For larger particles and nonstationary systems, measurements at smaller angles are mandatory. From the scaling of the scattered intensity one can obtain reliable information on the mean size and mass of the evolving structures and on the exponents and rates that typify the crystallization process.

In a classical SLS experiment the scattered light intensity is plotted as a function of the scattering vector **q**. The parameter of interest is the long-term time average of the scattered intensity $\langle I_s(q)\rangle$:

$$\langle I_s(q)\rangle = \lim_{T\to\infty}(1/T)\int_{t_0}^{t_0+T} I(q,t)\,\mathrm{d}t \qquad (1)$$

This average is independent of the time t_0 at which the measurement is initiated if $I(q,t)$ is a stationary property, which is normally the case. In the limit of infinite dilution and small scattering vectors, SLS measurements provide reliable values of the weight-average molecular weight and the mean squared radius of gyration $\langle R_g^2\rangle$.

Cyclodextrins under crystallization conditions are systems that suits these requirements. Pertinent information concerning the growth of microcrystals can be directly deduced from the small-angle SLS experiments. In this work crystallization was induced by cooling β-CD solutions below and by heating DIMEB above the nucleation temperature T_n. In either case the growth kinetics of mean size and mass of the formed nuclei can be followed as a function of the elapsed time after cooling or heating.

Nucleation from the Melt. The growth of crystals, which is a first-order phase transition,[9] can occur in one, two, or three dimensions, giving rise to rod-, disk-, or spherelike structures.[10] Changes in the linear dimensions of the crystallites are experimentally accessible with a variety of methods. The

* To whom correspondence should be addressed. Phone: +030-838-4588. Fax: +030-838-6702. E-mail: yannis@chemie.fu-berlin.de.

⊗ Abstract published in *Advance ACS Abstracts,* September 15, 1996.

(1) Frömming, K. H.; Szejtli, J. *Topics in Inclusion Sciences*; Kluwer Academic Publishers: Dordrecht, The Netherlands, 1994.
(2) Wenz, G. *Angew. Chem.* **1994**, *106*, 851.
(3) Saenger, W. *Isr. J. Chem.* **1985**, *25*, 43.
(4) Arad-Yellin, R.; Green, B. S. *Nature* **1994**, *371*, 320.
(5) Betzel, C.; Saenger, W.; Hingerty, B. E.; Brown, G. M. *J. Am. Chem. Soc.* **1984**, *106*, 7545.
(6) Steiner, T.; Saenger, W. *Carbonhydr. Res.* **1995**, *275*, 73.
(7) Szejtli, J. *Cyclodextrins and their Inclusion Complexes*; Akadémiai Kiadó: Budapest, 1982.
(8) Georgalis, Y.; Schüler, J.; Umbach, P.; Saenger, W. *J. Am. Chem. Soc.* **1995**, *117*, 9314.
(9) Oxtoby, D. W. *Adv. Chem. Phys.* **1988**, *70*, 263.
(10) Hurle, D. T. J., Ed. *Fundamentals of Crystal Growth, Thermodynamics and Kinetics*; North-Holland: Amsterdam, 1994.

S0002-7863(96)00567-7 CCC: $12.00

growth of the crystallites is expected to be linear in time, if the crystallization temperature T_c remains constant; *i.e.*, the mean radius $\bar{R}(t)$ of a spherical crystallite grows with a constant rate k_w:

$$\bar{R}(t) = k_w t \tag{2}$$

Equation 2 holds for crystallites that are still small and do not grow together, *i.e.*, only in the initial growth phase. For a certain compound the growth constant k_w depends on the crystallization temperature.[10]

A theory that describes the growth of crystallites from the melt (homogeneous crystallization) was developed by Avrami.[11−13] If one denotes as $m(0)$, $m(s)$, and $m(c)$ the masses of the monomeric seed, the mass of the melt, and the mass of the crystalline state, respectively, the following holds:

$$[m(c)/m(0)] = 1 - \exp(-k_A t^{n_A}) \tag{3}$$

where k_A denotes the Avrami constant, valid for spherical crystallites, and n_A the Avrami exponent.

Equation 3 is valid under a series of assumptions: (i) The amount of nuclei N_c is either constant or at the beginning of the crystallization equals zero and increases with constant rate k_w. (ii) The nuclei are distributed statistically in the examined sample. (iii) The density of the crystallites is always the same. (iv) The form the crystallite (*e.g.*, sphere) does not change as crystallization proceeds.

From the excperimental point of view it is easier to determine changes in the volume of the crystallites through dilatometry: Assuming that $v(0)$, $v(t)$ and $v(\infty)$ are the volumes of the probe at $t = 0$, t, and $t = \infty$, the following holds:

$$v(t) = \left[\frac{m(s)}{\rho(s)}\right] + \left[\frac{m(c)}{\rho(c)}\right] = \left[\frac{m(0)}{\rho(c)}\right] + m(s)\left[\frac{1}{\rho(s)} - \frac{1}{\rho(c)}\right] \tag{4}$$

where for the "melted" and crystalline states

$$v(0) = \left[\frac{m(0)}{\rho(s)}\right] \quad \text{and} \quad v(\infty) = \left[\frac{m(0)}{\rho(c)}\right] \tag{5}$$

In eqs 4 and 5 $\rho(c)$ and $\rho(s)$ denote the densities of the substance in the crystal and melt, respectively. It can be shown that

$$\left[\frac{v(t) - v(\infty)}{v(0) - v(\infty)}\right] = \exp(-k_A t^{n_A}) \tag{6}$$

Equation 6 contains only two unknowns, namely, k_A and n_A. Both can be determined by taking logarithms twice to obtain the linearized equation:

$$\ln[\ln(F)] = n_A \ln(k_A) + n_A \ln(t) \tag{7}$$

where $F = (v(0) - v(\infty))/(v(t) - v(\infty))]$. If a linear behavior is observed the y axis intercept is equal to $n_A \ln(k_A)$, and the slope to n_A. Equivalent information can be deduced if the volume scaling on time is replaced by the respective mass or size scaling deduced from time-resolved experiments. In such a case the mass-weighted crystallite mass at time t is taken to be proportional to the zero-angle extrapolated scattered intensity $I_s(0,t)$

$$I_s(0,t) \equiv m(t) \equiv R_g^3(t) \tag{8}$$

assuming a compact spherical shape. Both $m(t)$ and $R_g(t)$ can be independently determined from time-resolved small-angle SLS experiments. We have employed directly the proportionality between volume and mass to retrieve F, neglecting the small density differences expected for CDs in the liquid or crystalline state.

The significance of Avrami exponents higher than 3 can be understood in terms of scaling of the number of nuclei at the early stages of the phase transformation. If this rate is proportional to the first power of time but the respective volumes scale with the third power, an exponent of four is expected.

Materials and Methods

Purification of Cyclodextrins. β-CD was purchased from Sigma Chemicals Co. (lot 47F-3509). Since the solubility of β-CD in water at room temperature is only 19 mg/mL,[1,7] preweighted quantities of β-CD were dissolved in boiling, degassed triply distilled water and incubated for 10 min at 343 K. Samples examined by analytical HPLC were found to contain only β-CD.

DIMEB (lot 1039453) was purchased from Aldrich Chemicals and contained a strongly fluorescent compound. To remove this impurity, DIMEB was dissolved in water and active coal was added. After incubation for 20 min the active coal was removed by filtering and DIMEB was recrystallized by heating to 343 K; the crystallization procedure was repeated 10 times. Analytical HPLC has shown the presence of 10% unmethylated β-CD. The clear nonfluorescent DIMEB was lyophilized and used in the experiments described below. Further improvement on the purification involved a 3-fold recrystallization of DIMEB from water at 333−343 K and tedious collection of the needle-like crystals under a microscope. This preparation has been again checked by HPLC, and less than 3% β-CD was found in the samples. The differences determined between the two recrystallized preparations on the characteristic exponents via small-angle light scattering were found to be within less than 5%. Therefore, we can conclude that native β-CD does not appreciably influence the observations on crystallization kinetics of DIMEB. We should however, emphasize that under such narrow peaks a mixed population of β-CD molecules carrying other than 2,6-dimethylated glucoses may be hidden.

In the experiments described below β-CD was cooled from 343.2 to 308 K, whereas DIMEB was heated from 293.2 to 343.2 K to fuel crystallization. In either case, solutions were rapidly filtered through 800 μm pore size filters and measurements were initialized immediately because bothn cyclodextrins exhibit slow spontaneous growth kinetics even at concentrations below the solubility limit (own unpublished observation).

Small-Angle SLS. Small-angle SLS experiments were conducted employing a home-made apparatus. Scattered light is detected by an 8-bit CCD chip (Sony ICX 039, Cheops Co., Munich). After collimation the light passes through the sample and impinges on a mirror with a hole in the middle for isolating the primary beam at the forward direction. A typical 3.5 in. silicium wafer served as a mirror. Holes of variable diameter are required for some experiments, depending on the beam expansion and spot diameter of the detected scattered light. In its present configuration the effective angular range extends from 1.2° to 13.6° corresponding to scattering vectors between 2.8×10^{-4} and 3.1×10^{-3} nm^{-1} for the He−Ne wavelength, 632.8 nm. This angular range allows the examination of particle radii within the range of 300 nm and 5 μm. The instrument, with dimensions 60 cm × 60 cm, is mounted on an optical table (Newport) and covered with a light-tight box. Samples are injected to squared fluorescence cells placed in a thermostated holder, and temperature is stabilized to within 0.01 K by a Lauda RC6 thermostating unit. Sample path lengths may vary between 1 and 10 mm, depending on probe turbidity and multiple scattering. Devices similar to ours have been described also by other investigators[14−17] employing either CCD devices or reticons that enable detection of scattered light at small angles.

(11) Avrami, M. *J. Chem. Phys.* **1939**, *7*, 1103.
(12) Avrami, M. *J. Chem. Phys.* **1940**, *8*, 212.
(13) Avrami, M. *J. Chem. Phys.* **1941**, *9*, 177.
(14) Rouw, P. R.; Woutersen, A. T. J. M.; Ackerson, B. J.; de Kruif, C. G. *Physica A* **1989**, *156*, 876.

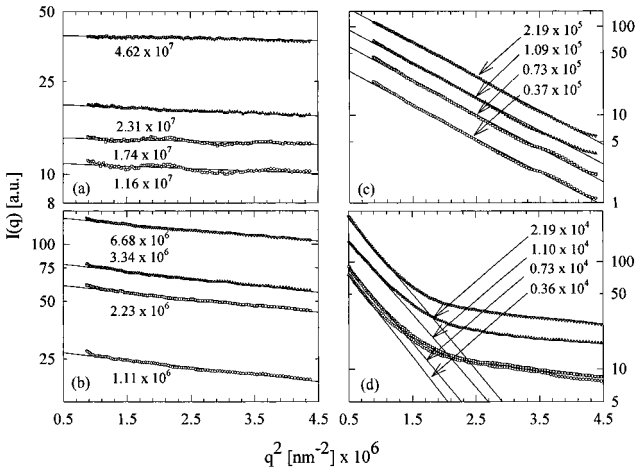

Figure 1. (a) Aqueous suspensions of Latex-Unispheres examined with the small-angle SLS apparatus. Nominal radii are (a) 274, (b) 477, (c) 1478, and (d) 3047 nm. The numbers of particles per milliliter are indicated for each curve. Scattering intensities are plotted according to eq 12, and the quoted mean particle sizes are deduced from extrapolation to infinite dilution (Table 1).

The scattered intensity is received by the CCD chip as a circular spot and stored temporarily as a bitmap. The acquisition of each bitmap requires less than 200 ms, and bitmaps were recorded with a frequency of 30 s each. After circular pixel averaging, the median values are stored sequentially as a function of the distance from the origin. The determination of the origin is made in advance with the cursor function using the maximum intensity of the naked laser beam for centering. The scattering vector calibration is accomplished by Fraunhofer diffraction through pinholes with known diameter, depending on the desired angular range. In the present work we used pinholes with $D = 30\ \mu$m, with the intensity minima of the diffraction pattern defined by $\sin(\theta) = 1.22\ (\lambda/D)$. The distance of each pixel from the origin is computed as a function of the scattering vector. Due to the low dynamic range of the CCD chip a bank of filters, with known transmission, is placed after the beam expander to avoid saturation of the CCD chip, and gray scale renormalization is accomplished under software control. The drivers for the overlay card and bitmap acquisition have been developed by Cheops. Their binding to pixel averaging, data formatting and storage, automated nonlinear evaluation routines for a Silicon Graphics workstation, etc. were performed by us.

Dilute aqueous suspensions of large Latex-Unispheres (Serva, Heidelberg) particles with nominal radii 273, 477, 1478, and 3047 nm were employed for the calibration, and correction of the CCD chip delivered values of the scattered intensities. The mean radii of those particles have been also determined by dynamic light scattering (DLS) following procedures described previously.[8] The conditions for Rayleigh−Debye scattering are[18]

$$|m - 1| \ll 1 \tag{9}$$

$$(2\pi/\lambda)R_0|m - 1| \ll 1 \tag{10}$$

$$I_s(q) \equiv |m - 1|^2\,(3\pi/(qR_0)^2)J_{3/2}{}^2 \tag{11}$$

where m is the ratio of refractive indices of the solute and solvent and $J_{3/2}$ is a Bessel function of fractional order. Latex particles have an index of refraction $n_L \approx 1.58$, and that for water at 293.2 K is $n_W = 1.334$. Particle sizing of very dilute aqueous Latex suspensions delivered values that are fairly close to the ones suggested by the manufacturer (Figure 1). In such comparisons deviations from the nominal values arise from sample polydispersity, interactions between particles, turbidity corrections, and multiple scattering.

Table 1. Comparison of the Mean Hydrodynamic Radii, R_h, of Aqueous Suspensions of Latex-Unispheres (nm) Determined by Small-Angle SLS and DLS

R_{nom}	R_h (DLS)	R_h (SLS)	R_{nom}	R_h (DLS)	R_h (SLS)
273	294 ± 10^a 324 ± 39^b	306 ± 5^c	1478	1397 ± 140^a 1338 ± 111^b	1442 ± 51^c
477	471 ± 28^a 517 ± 75^b	488 ± 10^c	3047	nd[e]	$2902 \pm 60^{c,d}$

[a] Sizes deduced from a fourth-order semilogarithmic expansion of the autocorrelation function. [b] Sizes deduced from CONTIN[20,21] analyses. The quoted uncertainties denote the mean of 20 independent determinations. [c] The quoted sizes represent values from four different concentrations extrapolated to infinite dilution. The uncertainties are deduced as the mean of 10 independent bitmaps averaged over 200 ms each. In the respective DLS experiments only the most dilute Latex solutions have been employed instead. [d] These particles exhibit pronounced polydispersity (3047 ± 950 nm) according to the manufacturer. Data recorded at larger angles indicate particles with mean radii between 400 and 500 nm. [e] nd = not determined since the size of the particles exceeds the capabilities of the DLS technique.

Scattered intensities are computed after circular averaging of the corresponding bitmaps, and $I_s(q)$ is plotted in a semilogarithmic fashion vs q^2 (Guinier type of plot):[19]

$$I_s(q) = I_s(0)\,\exp[1 - q^2R_g{}^2/3] \tag{12}$$

The intercepts from linear least-squares fits of the data, $I_s(0)$, can be obtained with adequate precision. The respective slopes can be directly associated with the radius of gyration of the particles, R_g, by linearizing eq 12. A comparison between the nominal radii values of the Latex particles as determined by DLS and small-angle SLS is given in Table 1.

The agreement between the nominal sizes quoted by the manufacturer and the ones determined through DLS and the small-angle SLS apparatus is satisfactory. We can thus conclude that our apparatus can capture particle sizes with good enough speed and precision to follow the kinetics of nonstationary processes.

Light Microscopy. Time-resolved images of 50 mg/mL aqueous DIMEB solutions were recorded with an Axiovert 100 inverted microscope (Zeiss, Germany). Experiments were conducted in thermostated quartz slide cells, with a path length of 1 mm, and a CCD camera was used for acquiring the images at preselected time intervals. Video image processing was done by using commercially available software from Silicon Graphics. This procedure allows time-resolved observations of the overall change of needle-like DIMEB crystals.

Results and Discussion

β-CD and DIMEB nucleation kinetics have been monitored with small-angle SLS in a series of experiments above (β-CD) and below (DIMEB) the nucleation temperature, T_n. In these experiments the concentration of the solute was varied between 25 and 80 mg/mL. In this range both cyclodextrins crystallize easily within a few hours. However, it has to be noted that for obtaining β-CD crystals one starts cooling slowly from 343 K to room temperature whereas for DIMEB the reverse procedure is followed. These effects have been experimentally verified by DLS and SLS; they will be given in detail in a forthcoming paper. We face, therefore, the very interesting problem of a complete reversion of the aggregation and concomitant crystallization kinetics for each CD form, due to the introduction of the methyl groups.

In this work we have analyzed the SLS data and deduced the critical crystallization exponents according to the Avrami theory of nucleation. If $R_g(t)$ and $m(t)$ are known from the SLS experiment, eq 7 can be recast in a convenient form that allows

(15) Carpineti, M.; Ferri, F.; Giglio, M.; Paganini, E.; Perini, U. *Phys. Rev. A* **1990**, *42* (12), 7347.
(16) Schätzel, K.; Ackerson, B. J. *Phys. Rev. Lett.* **1992**, *68* (3), 33.
(17) Schätzel, K.; Ackerson, B. J. *Phys. Rev. E* **1993**, *48* (5), 3766.
(18) Kerker, M. *The Scattering of Light*; Academic Press: New York, 1969.
(19) Glatter, O. In *Neutron, X-Ray and Light Scattering*; Lindner, P., Zemb, Th., Eds.; North-Holland: Amsterdam, 1991.
(20) Provencher, S. W. *Comput. Phys. Commun.* **1982**, *27*, 213.
(21) Provencher, S. W. *Comput. Comput. Phys. Commun.* **1982**, *27*, 229.

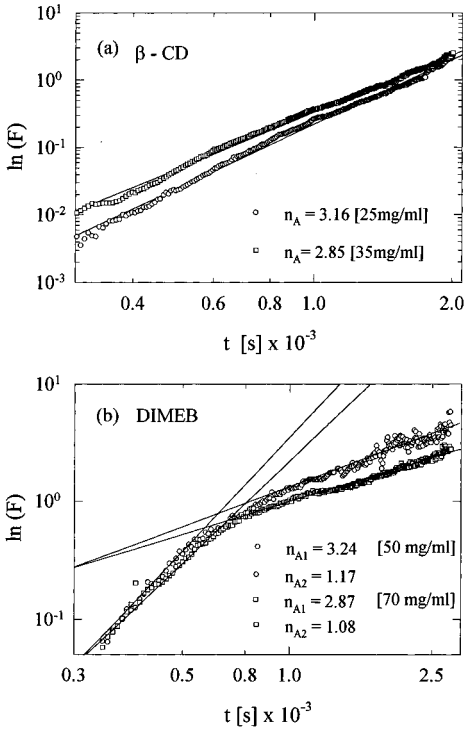

Figure 2. (a) Nuclei formation in aqueous β-CD solutions rapidly cooled from 343.2 to 308 K with concentrations of 25 and 30 mg/mL plotted according to eq 7. (b) Nuclei formation in aqueous DIMEB solutions rapidly heated from 293.2 to 343.2 K with concentrations of 50 and 70 mg/mL plotted according to eq 7. Note the biphasic character of the plots.

determination of the Avrami exponent n_A and the respective Avrami rate constant k_A from the recorded scattered intensities.

In Figure 2 we display double logarithmic plots of scattered intensities of records corresponding to temperature-quenched β-CD and DIMEB. Scattered intensities for times less than about 5 min are subject to large errors, and therefore, these regions have been deliberately neglected. We have also neglected small initial changes of the scattered intensity at times that have been attributed to thermal equilibration of the samples. Such changes are manifested through the sensitive dependence of refractive index on temperature. The data have been transformed according to eq 7, using as observable the zero-angle extrapolated scattered intensity, $I_s(0)$.

We have analyzed a large set of data on β-CD with the simple linear model and plotted the results as a function of the initial β-CD and DIMEB concentration to obtain both the nucleation exponent and rate constant at the infinite dilution limit. The plots of β-CD appear linear throughout, Figure 2a. In the concentration range between 20 and 80 mg/mL we obtained values for n_A that range between 4 and 1 (Figure 3a). They exhibit an exponential concentration dependence and could be fit with the function

$$n_A(c) = (5.68 \pm 0.09)\exp[-(0.023 \pm 0.002) \times c] \quad (13)$$

In their majority the data exhibit a close to t^1 to t^4 dependence on time, according to eq 7. The intercept in Figure 3a indicates that in the infinite dilution limit $n_A = 5.68$. This value is well above 4.00 which is taken as the upper limit for the crystallization exponent[11−13] of spherical crystallites. The reasons for such discrepancies are discussed below. The Avrami rate constant, k_A, exhibits a nearly sigmoidal behavior (Figure 3b). The transition time, Figure 4c, between the two processes depends on the initial concentration as would be expected for

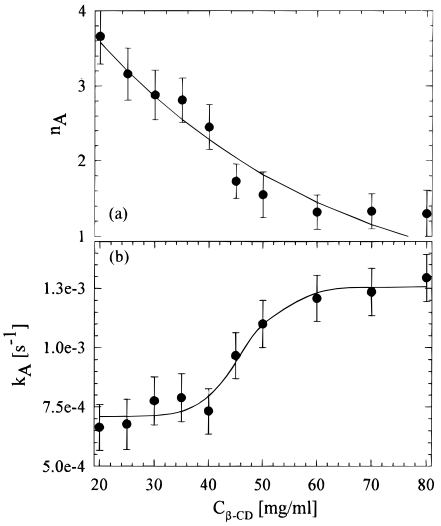

Figure 3. (a) Avrami exponents, n_A, and (b) Avrami rate constants, k_A, plotted as a function of β-CD concentration using weighted nonlinear fits. Note the decay of the Avrami exponent and the sigmoidal trend of the respective rates as a function of the initial β-CD concentration.

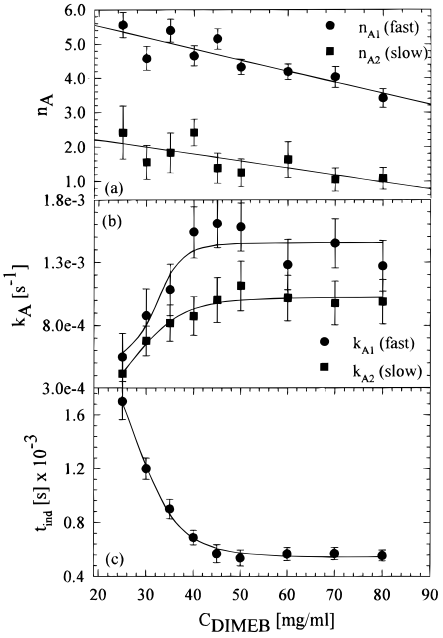

Figure 4. (a) Avrami exponents, n_A, (b) Avrami rate constants, k_A, and (c) time of appearance of the slow process plotted as a function of DIMEB concentration using weighted nonlinear fits. The dependence of the exponent on DIMEB concentration is to a good approximation linear. The trend of the Avrami rates and of the time of appearance of the slow process can be described as a simple logistic function of the initial DIMEB concentration.

an induction time.[10] This transition time increases almost linearly with concentration in the range between 40 and 60 mg/mL and remains constant around 1.3×10^{-3} s^{-1} for higher concentrations.

Pronounced differences are evident upon comparison of the native β-CD with DIMEB. In Figure 2b are depicted typical double logarithmic plots according to eq 7. Deviations from simple linear behavior were found in all SLS records collected with DIMEB. We interpret this biphasic behavior by invoking the presence of a fast and a slow process. The fast process is characterized by Avrami exponents in the range between 3.24 and 2.87 for the concentrations of 50 and 70 mg/mL and indicates the growth of spherical nuclei. After the transition time the shape of the nuclei changes as shown by the respective

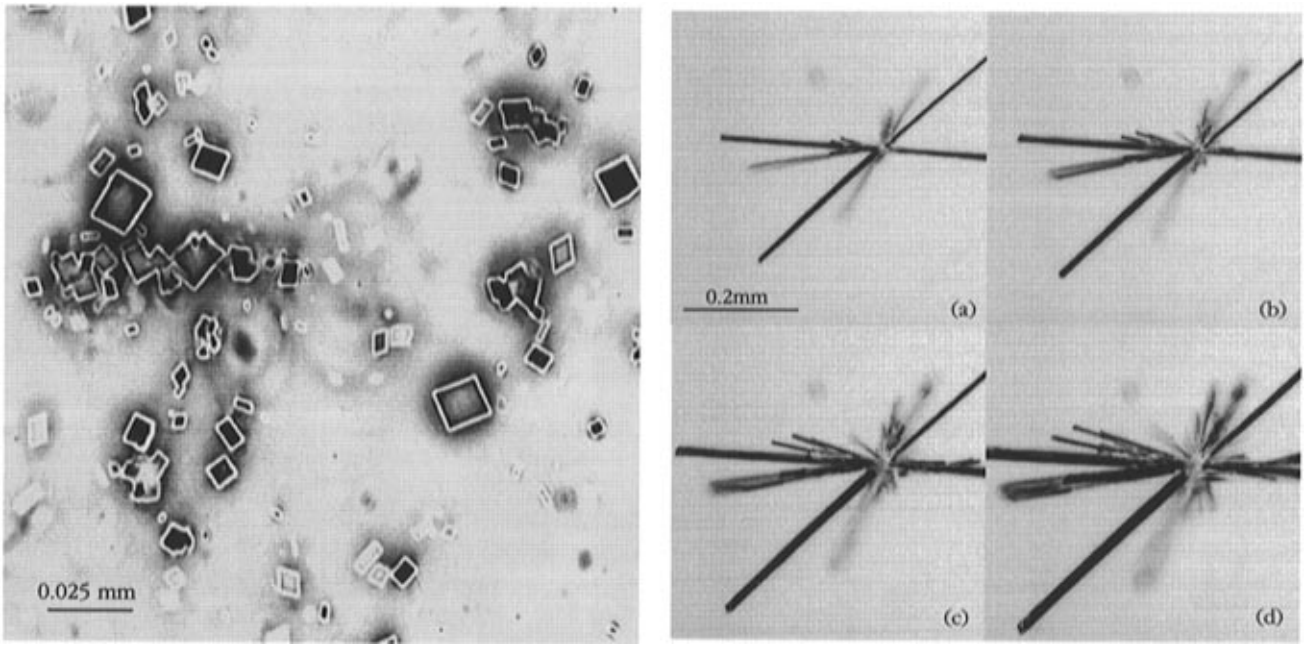

Figure 5. Light microscopy video records of (left) β-CD crystals at 293.2 K and (right) DIMEB crystals at 338.2 K upon completion of the SLS experiment with initial concentration, in both cases, 50 mg/mL. The needle-shaped DIMEB crystals that appear after 11 min have been further employed for extracting approximate macroscopic growth rates (see Figure 6).

Avrami exponents around 1.1 which could typify rodlike nuclei, Figure 4b. The latter was observed in the majority of the experiments (see discussion below).

We have extracted the Avrami exponents and rate constants by examining the linear regions of each data segment. Both exponents exhibit, within experimental error, a linear dependence on DIMEB concentration (Figure 4a); the data do not allow for more complex dependencies:

$$\{n_A(c)\}_{fast} = (6.07 \pm 0.35) - (0.033 \pm 0.006) \times c \quad (14)$$

$$\{n_A(c)\}_{slow} = (2.60 \pm 0.46) - (0.022 \pm 0.008) \times c$$

In their majority the data for the fast process indicate a t^4 to t^6 dependence on time, whereas those of the slow process support a t^1 to t^2 growth. At the infinite dilution limit we obtained $n_{A1} = 6.07$ for the fast process and $n_{A2} = 2.60$ for the slow process. The apparent crystallization rates, k_{A1} and k_{A2}, remain constant above 45 mg/mL. Finally we note that the slow process is initiated at times t_{ind} that show a nearly linear dependence in the concentration range below 45 mg/mL DIMEB and then remain constant.

The observed concentration dependence of the Avrami exponent could help to interpret several ambiguities in the variation of exponents observed in the contemporary literature. Further, the theory of nucleation[9,10] predicts extremely large changes of the nucleation rates for small changes of the concentration. However, such a behavior is not observed with CDs, and only moderate nucleation barriers are expected. This has been verified experimentally in our previous work[8] on aqueous solutions of β-CD where we have shown that the energetic barrier is rather low due to the heterogeneous crystallization.

Conclusions

We have shown that simple and inexpensive small-angle SLS equipment can be employed for time-resolved studies of aggregation and especially crystallization processes. The study of simple systems, where crystal formation is induced by temperature changes, is promising, and the characteristic crystallization exponents of both β-CD and DIMEB could be derived with adequate precision.

The various problems faced in our previous work on β-CD[8] are even more pronounced in the study of DIMEB due to the smaller angular range covered by the small-angle SLS apparatus. A major problem is the exact control of the size of the primary seed particles. Using dynamic light scattering, we have determined for both CDs mean cluster radii that range between 100 and 200 nm; *i.e.*, the initial particle size distribution is not well defined. Further, due to the heterogeneous nature of the nucleation, uncontrolled growth of microcrystals on the walls of scattering cells disturb the bitmaps or even render experiments impossible.

Problems are also associated with the determination of the Avrami exponents. Usually, one finds for the Avrami exponent n_A values that lie between 1 and 6, more often between 3 and 4. Some of the causes for the deviations of the experimental results from the theoretically expected values can be summarized: (i) $v(\infty)$ is not exactly definable, and it is frequently unclear whether the crystallization is already finished or still proceeds. (ii) Secondary crystallization may take place; the crystallinity of the solid phase already formed may then strongly increase. (iii) Heterogeneous impurities may cause additional nucleation that cannot be controlled. (iv) Regions of the solution that are unable to crystallize reduce the total crystal growth velocity; the predictions of the Avrami theory are in practice only partially fulfilled. The real causes for the numerous deviations are to a large extent unknown.

The growth of β-CD crystals follows a rather simple mechanism as predicted by the classical nucleation theory[22−24] and results in compact macrocrystals as depicted in Figure 5a. The growth of DIMEB crystals is by far more complex. It involves an initial formation step with an Avrami exponent characteristic of spherical particles. After a certain, concentration dependent induction time, t_{ind}, DIMEB crystals grow into

(22) Russel, W. B. *Phase Transitions* **1990**, *21*, 127.
(23) Wagner, C. *Z. Elektrochem.* **1961**, *65* (7/8), 581.
(24) Gunton, J. D.; San Miguel, M.; Sahni, P. S. In *Phase Transitions and Critical Phenomena*; Domb, C. Lebowitz, J. L., Eds.; Academic Press: New York, 1988; Vol. 8, p 267.

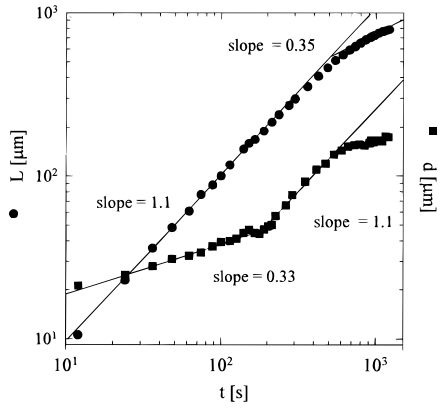

Figure 6. Typical growth of length *L* and diameter *d* of a single needle-like DIMEB crystal at 338.2 K. Note that the exponents characterizing axial and radial growth reverse after 200 s and that the sizes attained during axial growth are nearly an order of magnitude larger than those of radial growth.

elongated rods as indicated by a change in the Avrami exponent and as shown by microphotography, Figure 5b.

The DIMEB crystals appear suddenly in solution when the temperature approaches 335 K and grow very fast to macroscopic dimensions, above 1 mm. Crystallization ceases within a few minutes, but within macroscopic time scales is fully reversible. This effect contrasts the behavior of DIMEB in temperature gradients where a very pronounced hysteresis between heating and cooling cycles is observed by small-angle SLS (own unpublished observation).

Video image analysis of selected crystals indicates a power law growth of the diameter and length of DIMEB crystals. A typical plot of these results with the exact exponents is displayed in Figure 6. Length and diameter growth follows power laws such as $L \approx t^{1.1}$ and $d \approx t^{0.33}$ that reverse at later stages to $L \approx t^{0.35}$ and $d \approx t^{1.1}$. From the overall trend it seems that radial and axial accumulation of DIMEB onto the crystal are two competing processes.

One can determine the macroscopic rate constant for the growth of such needle-shaped crystals using the microphotographic observations. We can then deduce the approximate axial growth rate for the DIMEB crystals assuming that radial growth of crystals is much slower than axial growth. For DIMEB at 341 K this rate is *ca.* $(6.7 \pm 1.2) \times 10^8$ DIMEB monomers per s and μm^2 and, as expected, slightly lower, $(5.1 \pm 0.8) \times 10^8$ DIMEB monomers per s and μm^2, at 338 K. It should be mentioned that reduced rates obtained from the scaling of the submicrometer clusters radii on time, eq 2, as determined by SLS, are 4 orders of magnitude lower than these figures.

In summary we have shown that small-angle SLS is a useful method for rapidly extracting meaningful information on heterogeneously crystallizing systems. In first-order phase transitions the coupling among density, energy, and the crystal order parameter is very complex and has been investigated only for very simple homogeneously nucleating systems.[17,18] Although the nucleation of CDs is not homogeneous, the attained agreement with current phenomenological approaches, which are valid for hard uncharged spheres, is satisfactory and can be employed as a first platform. The complete reversion of the aggregation behavior of DIMEB in comparison with native β-CD is a noteworthy effect that signifies the character of the interactions between CD molecules. The development of an adequate theoretical description to explain this effect will be necessary. Further experimental work for elucidation of the crystallization dynamics of CDs is underway in our laboratory.

Acknowledgment. Financial support to Y.G. from the Deutsche Forschungsgemeinschaft (Grant Sa 196/26-1) and to P.U. from the DESY 05 641KEB project is acknowledged. We also thank Mr. E. Rümenapf for his help in machining parts of the SLS apparatus, Mr. W. Lamers for conducting the analytical HPLC runs, and Professor K. Galicki for helping us obtain several unavailable books.

JA9605679